Oxygen in antimony triselenide: an IR absorption study

F. Herklotz,[1] E. V. Lavrov,[1] T. D. C. Hobson,[2] J. D. Major,[2] and K. Durose[2]
[1)]*Technische Universität Dresden, 01062 Dresden, Germany*
[2)]*Stephenson Institute for Renewable Energy, University of Liverpool, Liverpool L69 7ZF, UK*

(*Electronic mail: frank.herklotz1@tu-dresden.de)

(Dated: April 11, 2022)

Oxygen in single crystalline antimony triselenide (Sb_2Se_3) is addressed by infrared (IR) absorption spectroscopy. Measurements conducted on Sb_2Se_3 samples doped—during growth, post-growth annealing in the O_2 ambient, or by O ion implantation— with ^{16}O reveal an IR absorption line at 527 cm^{-1} (10 K). Substitution of ^{16}O by ^{18}O 'red'-shifts the signal down to 500 cm^{-1} based on which the line is assigned to a local vibrational mode of an isolated oxygen defect. Annealing of O-enriched samples in hydrogen atmosphere at temperatures above 380 °C results in the suppression of the 527-cm^{-1} line and concurrent appearance of the signals due to hydroxyl groups, suggesting formation of oxygen-hydrogen complexes. The configuration of the 527-cm^{-1} oxygen center is discussed.

Oxygen plays an important role as key contaminant in many solids. Its decisive impact on the performance of various semiconductor devices has attracted considerable research interest over the decades leading to identification of fundamental microscopic configurations of oxygen defects in the host lattice and revealing their electrical activity.

Silicon is a classic example of a material where spectroscopic studies of various kinds in combination with first principles theory led to profound understanding of oxygen-related defects.[1] Oxygen on interstitial sites *dynamically* occupies a bond-centred location between its two nearest-neighbor Si atoms. The Si−O−Si 'molecule' gives rise to a strong IR active antisymmetric stretch mode at ∼1136 cm^{-1} (10 K).[2,3] Interstitial oxygen in silicon does not have a level in the band gap. It forms, however, electrically active complexes with other impurities and defects in the course of device processing. By far the most important example is thermal donors formed during low-temperature treatment in the range 300–500 °C.[1] Notably, despite an overwhelming number of studies dealing with these donors, the atomic structure and the origin of the electrical activity are still not well understood.[4,5]

Oxygen has also been extensively studied in GaAs due to its role as a deep-level defect. In this material, O forms two distinct centers with unique vibrational mode spectra: An interstitial species bond-centred between neighboring Ga and As atoms (845 cm^{-1} line), and a substitutional center (V_{As}–O) in which O is located slightly off-centered primarily binding to two of its Ga neighbors (715 cm^{-1}).[6] Further examples where the nature of fundamental oxygen species has been established include GaP,[7] CdTe,[8–10] ZnTe,[11] and CdSe.[10]

The present work addresses antimony triselenide (Sb_2Se_3)—an emerging chalcogenide semiconductor material considered as a promising photovoltaic absorber. It possesses an unique orthorhombic quasi-1-dimensional crystal structure in which covalently bonded $[Sb_4Se_6]_n$ 'nano-ribbons' are linked by weak van der Waals interaction.[12,13] Research related to the role of oxygen in this material started quite early, after it has been recognized that oxygen doping has a strong influence—a combination of both beneficial and detrimental aspects—on the performance of Sb_2Se_3 thin film solar cells (see, e.g., Refs. 14–18). Characterization of oxygen as a key contaminant in such devices is of particular importance since unintentional in-diffusion of this element may occur well below typical growth and/or processing temperatures. A number of studies have applied X-ray photoelectron (XPS) and Raman spectroscopies to detect antimony oxide impurity phases (Sb_2O_3, SbO_2, Sb_2O_5) in Sb_2Se_3.[17,19–22] Yet, experimental pieces of evidence for fundamental *isolated* oxygen species in this material are unknown.

Theory predicts several possible intercalation sites for oxygen in Sb_2Se_3.[15,16,21] Substitutional oxygen on different selenium sites (O_{Se}) was found to have very low formation energy. O_{Se} does not have a level in the band gap, thus not contributing to the conductivity of Sb_2Se_3. More importantly, oxygen passivates the anion vacancies, which act as recombination centers in Sb_2Se_3 due to their mid-gap states (see, e.g., Ref. 23). Oxygen was also found to potentially occupy a variety of interstitial sites (O_i) located either within the large van der Waals voids[16,21] or bonding with Sb and Se atoms within the same ribbon, i.e., forming a Sb-O-Se chain.[21] These centers have relatively low formation energies and are also electrically inactive. The calculated migration barrier of O_i along the dominant van der Waals channels of Sb_2Se_3 was found to be 1.0 eV, implying that interstitial oxygen is mobile at typical device processing temperatures.[21] A complex consisting of O_{Se} located next to a Sb vacancy was also considered.[15] Interestingly, it was found that this complex has a low formation energy with an acceptor level shallow enough to provide effective *p*-type conductivity.

The aim of this Letter is identifying fundamental isolated oxygen defects in antimony triselenide. Our infrared absorption measurements on O-doped bulk single-crystalline Sb_2Se_3 samples show that a vibrational mode at 527 cm^{-1} (10 K) can be unambiguously assigned to an oxygen center. Its possible microscopic configuration is discussed.

Single-crystalline Sb_2Se_3 samples grown by a vertical Bridgman melt-growth method were used in our study. Details of crystal growth can be found in Refs. 24 and 25. The crystals had diameter up to 4 mm with a length of 1 to 3 cm. Subsequently, they were cleaved, cut, and polished to prepare (010)-oriented samples (*Pbnm* space group nomenclature) with a front size of about 3×3 mm^2.

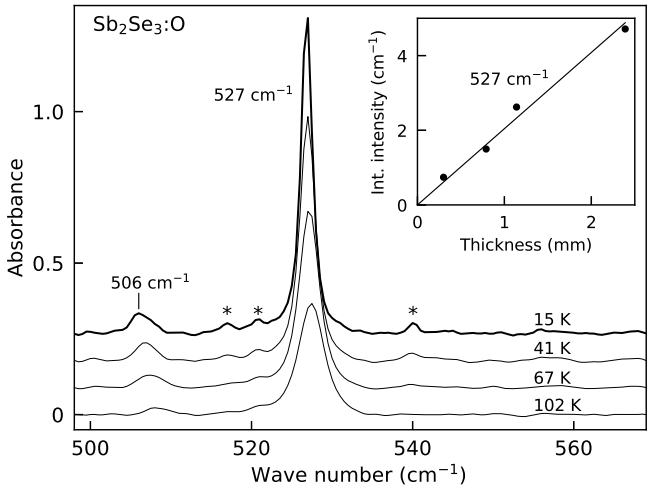

Figure 1. Infrared absorption spectra obtained at different temperatures for an exemplary in-growth O-doped Sb_2Se_3 sample. Spectra are offset for clarity. Inset shows integrated intensity of the 527 cm^{-1} mode vs. sample thickness obtained within a series of stepwise polishing treatments.

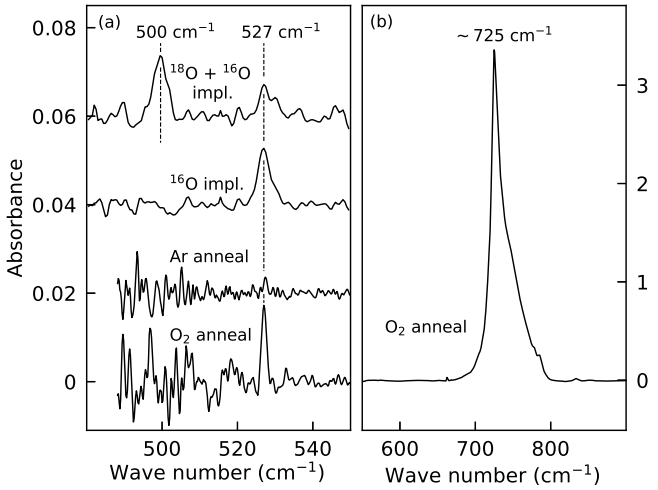

Figure 2. (a) IR absorption spectra recorded on Sb_2Se_3 samples subjected to four different post-growth treatments. From top to bottom: ^{18}O- and ^{16}O-ion implantation to the fluences of 13.5×10^{15} and 9×10^{15} cm^{-2}, respectively; ^{16}O-ion implantation to the fluence of 11×10^{15} cm^{-2}; anneal in Ar ambient at 230 °C for 1 h; anneal in O_2 ambient at 230 °C for 1 h. (b) Expanded section of the spectrum taken on the O_2 annealed sample.

Three methods of were employed to introduce oxygen: (i) in-growth doping, (ii) in-diffusion from the O_2 gas ambient, and (iii) ion implantation. In the first procedure, the ampules for the Bridgman growth were sealed with a small quantity of Sb_2O_3 powder, corresponding to (0.1 ± 0.01) at% of the Sb_2Se_3 source material. The two powders were ground together to aid incorporation of O during growth. For the nominally oxygen free "reference" Sb_2Se_3 samples, only Sb_2Se_3 powder was used. In both cases, ampules were sealed under ∼100 mbar Ar ambient at 300 K to suppress vaporisation and promote melting. For post-growth oxygen in-diffusion treatments, labeled here as O_2 "anneal", reference samples were sealed in quartz ampules filled with 400 mbar oxygen gas at room temperature, and subjected to a thermal treatment at 150–250 °C for 1 h. Ion implantations with ^{18}O and/or ^{16}O ions were performed at the Ion Beam Center of Helmholtz-Zentrum Dresden-Rossendorf (HZDR), Germany. The implantations consisted of a multi-step sequence with ion energies of 3, 1.6, 0.8, and 0.5 MeV and total dose in the range of 0.25–1.8 $\times10^{16}$ cm^{-2}.

Infrared absorption spectra were recorded with a Bomem DA3.01 Fourier transform spectrometer equipped with a globar light source, a KBr beam splitter, and a liquid nitrogen cooled MCT detector. The measurements were performed in a He exchange-gas cryostat equipped with either KBr or polyethylene windows, with the temperature of the samples stabilized within 2 K. Unless noted otherwise, measurements were taken at ∼10 K. The spectral resolution was 0.4–1.2 cm^{-1}.

Figure 1 shows IR absorbance spectra obtained for an exemplary in-growth O-doped Sb_2Se_3 sample. The spectra reveal a dominant absorption line at 527 cm^{-1}. The feature broadens and slightly 'blue'-shifts with the temperature, which indicates the vibrational nature of this line. A minor peak at ∼506 cm^{-1} as well as at least three other weaker features, marked by stars, are further seen in the spectra. These signals also shift and broaden with the temperature. In the present work, we focus on the dominant 527 cm^{-1} line as the weakness in intensity renders detailed investigations and conclusion on the minor features challenging. The entirety of our data, however, suggest a common microscopic nature or kinship in defect chemistry since all lines seen in the figure occur simultaneously.

In order to verify if the 527-cm^{-1} line originates from the bulk of the in-growth doped samples, we performed IR absorption measurements within a series of sequential polishing steps which gradually reduced the sample thickness from about 2.4 to 0.3 mm. The results are shown in the inset of Fig. 1. The linear dependency of the 527-cm^{-1} line intensity on the sample thickness clearly demonstrates that the defect of interest is homogeneously distributed over the sample depth.

The 527-cm^{-1} peak dominates the spectra of all in-growth O-doped Sb_2Se_3 samples, whereas the signal is either very weak or absent in all "reference" samples. Such a behavior is clearly in favor of oxygen as a main constituent of the defect responsible for the 527-cm^{-1} line. In order to verify this assumption, we performed post-growth doping of nominally oxygen-free Sb_2Se_3 samples. Fig. 2 shows "differential" absorbance spectra whose references were recorded before the corresponding treatment took place. The features seen in the spectra thus inherently reflect changes caused by the corresponding treatment.

The upper two spectra in Fig. 2(a) were recorded on two different Sb_2Se_3 samples implanted with ^{16}O and ^{18}O+^{16}O ions. As one can clearly see, implantation with the pure ^{16}O isotope species gives rise to the 527-cm^{-1} peak. The combination of both, ^{18}O and ^{16}O, ions results in the appearance of the 527-cm^{-1} mode *and* an additional signal at ∼500 cm^{-1}.

The frequency ratio of the two lines, $499.5/527.3 = 0.9473$, corresponds well to the value expected for local vibrational modes of ^{18}O and ^{16}O impurities, $\sqrt{16/18} = 0.9428$. Moreover, the relative intensities of the two modes match those of the ^{16}O and ^{18}O ion fluences used for implantation (see figure caption). These observations strongly suggests that the 527- and 500-cm^{-1} modes are due to isotopic ^{16}O and ^{18}O varieties of a common isolated oxygen defect species.

The lower two spectra in the figure were taken on samples after annealing in Ar and O_2 ambient at 230 °C. The oxygen treatment gives rise to the 527-cm^{-1} line, whereas in the case of argon the signal is practically missing. These findings provide further strong support for the involvement of oxygen in this defect.

We note that the O_2 annealing procedure at 230 °C produces a rough layer at the sample surface which is absent in case of implantation or if the treatment temperature is below 200 °C. In the latter case, the 527-cm^{-1} line does not appear in the spectra either. For temperatures above 250 °C, the surface layer is so intense that quantitative IR measurements are rendered impossible due to significant scattering and low IR signal intensity related thereto.

We attribute the rough layer to Sb_2O_3 formed by surface oxidation of Sb_2Se_3. Evidence for such an assignment is presented in Fig. 2(b), which shows an expanded section of the spectrum recorded on the O_2 annealed sample. The spectrum reveals an intense broad band at about 725 cm^{-1} which closely matches the value of the dominant T_2-like Sb−O−Sb stretch mode of α-Sb_2O_3 (see Refs. 26 and 27). This peak is uniquely seen as a result of O_2 annealing procedures and correlates with the apparent roughness of the surface layer. Removing the layer by lapping and polishing eliminates the 725-cm^{-1} band. At the same time such a procedure also results in disappearance of the 527-cm^{-1} line. These findings demonstrate that exposure of Sb_2Se_3 to oxygen may cause both, the formation of surface-near Sb_2O_3 phases and 527 cm^{-1} centers.

Figure 3 presents results of an isochronal annealing series carried out in a mixture of H_2 and D_2 gas for an in-growth O-doped Sb_2Se_3 sample. The main figure shows a selection of exemplary absorption spectra obtained after different treatment steps, whereas the inset gives the intensity of the 527-cm^{-1} mode as a function of the annealing temperature. It can be seen that the 527-cm^{-1} defect anneals out between 350 and 420 °C. Interestingly, the H_2/D_2 treatments at such temperatures also give rise to a number of new lines with frequencies in the spectral ranges of about 2550−2600 and 3430−3490 cm^{-1}, characteristic of stretch vibrations of O−D and O−H groups, respectively. Similar treatments performed for nominally O-free reference samples do not result in the hydroxyl stretch modes. Such a behavior can be understood if we assume that hydrogen/deuterium gets trapped by oxygen released from the 527-cm^{-1} defect in cause of the thermal treatment. Properties of the O−H/O−D centers are beyond the scope of this study and will be the topic of the future investigations.

The bulk of our experimental data strongly suggest that the defect responsible for the 527 cm^{-1} line includes a single oxygen atom. As mentioned in the introduction, recent first-principles studies consider a number of intercalation sites of oxygen atoms in Sb_2Se_3.[15,16,21] These works consistently find that formation of O_{Se_n} ($n = 1,2,3$) centers is energetically favorable and, thus, can account for the 527-cm^{-1} mode. Among the quasi-1-dimensional Sb_4Se_6 ribbons of Sb_2Se_3 there are three symmetrically inequivalent Se sites. The calculations suggest that the center with O replacing the Se atom at the corner of the Sb_4Se_6 units (O_{Se_1}) has the lowest formation energy.[21] In this configuration, the O atom is covalently bound to one Sb atom of the same Sb_4Se_6 unit and loosely bound by van der Waals forces to second- and third-nearest Sb atoms located in adjacent Sb_4Se_6 units.[12,13,28] On the basis of the theoretical findings, we tentatively assign the 527-cm^{-1} line to the stretch mode of the strong covalent Sb−O bond of O_{Se_1}. However, the difference in formation energies of different O_{Se_n} centers is relatively low, implying that all of them may coexist. Minor modes at 506 cm^{-1} etc. seen in Fig. 1 are in favor of this assumption. Calculations on the vibrational frequencies of the O_{Se_n} centers would provide valuable means to verify these suggestions.

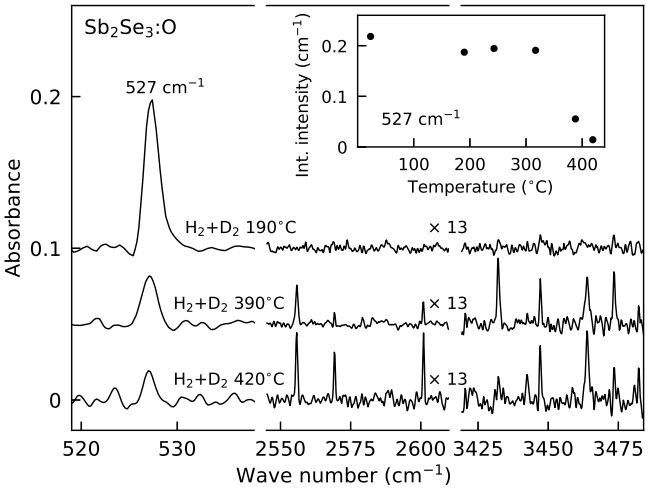

Figure 3. Results obtained on an in-growth O-doped Sb_2Se_3 sample in a series of isochronal treatments in H_2+D_2 ambient for 1 h. Main figure: Sections of IR absorption spectra recorded after annealing at 190, 390, and 420 °C. Inset: Integrated intensity of the 527-cm^{-1} mode as a function of the annealing temperature.

Oxygen may also occupy interstitial sites, either connecting adjacent Sb_4Se_6 ribbons or forming Sb−O−Se bonds within the same Sb_4Se_6 chain.[16,21] Both configurations take advantage of the roomy van der Waals voids of Sb_2Se_3 which offer large space for potential O intercalation. The shortest distance between Se and Sb atoms bridging the van der Waals gaps between adjacent ribbons is ∼3.47 Å,[12,13] much larger than typical Sb−O and Se−O bond lengths. The calculated formation energy of such interstitial centers is relatively low, which makes them further candidates to be considered as an origin of the 527-cm^{-1} line. Without detailed knowledge of the configuration and vibrational properties of O_i from first-principles theory, however, these suggestion remains speculative.

In recent years, XPS and Raman spectroscopy have been applied to study the impact of oxygen on Sb_2Se_3 devices.[17,20–22] These works address oxide impurity phases, such as Sb_2O_3, SbO_2, and Sb_2O_5, but do not provide insight into isolated O impurity centers. The formation of native oxide phases and that of the 527-cm^{-1} defect generally depend on the chemical potential of oxygen, and thus on the experimental conditions during growth and/or processing of Sb_2Se_3. Our findings demonstrate that the 527-cm^{-1} center and the Sb_2O_3 phase may coexist. We speculate that the former defect acts as "precursor" for the growth of native oxide, though this suggestion calls for a thorough verification.

In summary, an oxygen-related vibrational mode at 527 cm^{-1} in Sb_2Se_3 was studied by IR absorption spectroscopy. Substitutional oxygen at a selenium site or interstitial oxygen are proposed as likely origin of the 527-cm^{-1} mode. Our observations on an isolated oxygen center in Sb_2Se_3 are a complement to earlier X-ray photoelectron and Raman spectroscopy measurements addressing antimony oxide impurity phases in this material.

ACKNOWLEDGMENTS

TDC Hobson and JD Major acknowledge support from the Engineering and Physical Sciences Research Council via grants EP/N014057/1 and EP/T006188/1. We thank the Ion Beam Center of HZDR for ion implantations.

DATA AVAILABILITY STATEMENT

The data that support the findings of this study are available from the corresponding author upon reasonable request.

REFERENCES

[1]H. Bender and J. Vanhellemont, *Handbook on Semiconductors*, 2nd ed., edited by S. Mahajan, Vol. 3 (North-Holland, Amsterdam, 1994).
[2]W. Kaiser, P. H. Keck, and C. F. Lange, "Infrared absorption and oxygen content in silicon and germanium," Phys. Rev. **101**, 1264 (1956).
[3]H. J. Hrostowski and R. H. Kaiser, "Infrared absorption of oxygen in silicon," Phys. Rev. **107**, 966 (1957).
[4]B. Pajot, H. Compain, J. Lerouille, and B. Clerjaud, "Spectroscopic studies of 450 °C thermal donors in silicon," Physica B+C **117–118**, 110 (1983).
[5]J. A. Griffin, H. Navarro, J. Weber, L. Genzel, J. T. Borenstein, J. W. Corbett, and L. C. Snyder, "The new shallow thermal donor series in silicon," J. Phys. C **19**, L579 (1986).
[6]J. Schneider, B. Dischler, H. Seelewind, P. M. Mooney, J. Lagowski, M. Matsui, D. R. Beard, and R. C. Newman, "Assessment of oxygen in gallium arsenide by infrared local vibrational mode spectroscopy," Appl. Phys. Lett. **54**, 1442 (1989).
[7]P. J. Dean, M. S. Skolnick, C. Uihlein, and D. C. Herbert, "New aspects of the oxygen donor in gallium phosphide," J. Phys. C Solid State **16** (1983), 10.1088/0022-3719/16/11/007.
[8]G. Chen, I. Miotkowski, S. Rodriguez, and A. K. Ramdas, "Stoichiometry driven impurity configurations in compound semiconductors," Phys. Rev. Lett. **96**, 035508 (2006).
[9]E. Tarhan and A. K. Ramdas, "Local vibrational modes of natural isotopes of substitutional oxygen in CdTe," Turk. J. Phys. **44**, 247 (2020).
[10]F. Herklotz, S. Thiede, and E. Lavrov, "Vibrational signatures of substitutional oxygen in CdTe and CdSe," Phys. Status Solidi B **258**, 2100203 (2021).
[11]J. L. Merz, "Isoelectronic oxygen trap in ZnTe," Phys. Rev. **176**, 961 (1968).
[12]N. W. Tideswell, F. H. Kruse, and J. D. McCullough, "The crystal structure of antimony selenide, Sb_2Se_3," Acta Crystallogr. **10**, 99 (1957).
[13]G. P. Voutsas, A. G. Papazoglou, P. J. Rentzeperis, and D. Siapkas, "The crystal structure of antimony selenide, Sb_2Se_3," Z. Krist.-Cryst. Mater. **171**, 261 (1985).
[14]X. Liu, C. Chen, L. Wang, J. Zhong, M. Luo, J. Chen, D.-J. Xue, D. Li, Y. Zhou, and J. Tang, "Improving the performance of Sb_2Se_3 thin film solar cells over 4% by controlled addition of oxygen during film deposition," Prog. Photovoltaics **23**, 1828 (2015).
[15]H. Guo, Z. Chen, X. Wang, Q. Cang, X. Jia, C. Ma, N. Yuan, and J. Ding, "Enhancement in the efficiency of Sb_2Se_3 thin-film solar cells by increasing carrier concertation and inducing columnar growth of the grains," Solar RRL **3**, 1800224 (2019).
[16]L. Guo, B. Zhang, S. Li, A. Montgomery, L. Li, G. Xing, Q. Zhang, X. Qian, and F. Yan, "Interfacial engineering of oxygenated chemical bath–deposited CdS window layer for highly efficient Sb_2Se_3 thin-film solar cells," Mater. Today Phys. **10**, 100125 (2019).
[17]N. Fleck, O. S. Hutter, L. J. Phillips, H. Shiel, T. D. C. Hobson, V. R. Dhanak, T. D. Veal, F. Jäckel, K. Durose, and J. D. Major, "How oxygen exposure improves the back contact and performance of antimony selenide solar cells," ACS Appl. Mater. Inter. **12**, 52595 (2020).
[18]L. Wang, M. Luo, S. Qin, X. Liu, J. Chen, B. Yang, M. Leng, D.-J. Xue, Y. Zhou, L. Gao, H. Song, and J. Tang, "Ambient $CdCl_2$ treatment on CdS buffer layer for improved performance of Sb_2Se_3 thin film photovoltaics," App. Phys. Lett. **107**, 143902 (2015).
[19]A. Shongalova, M. R. Correia, B. Vermang, J. M. V. Cunha, P. M. P. Salomé, and P. A. Fernandes, "On the identification of Sb_2Se_3 using Raman scattering," MRS Commun. **8**, 865 (2018).
[20]C. Chen, Y. Zhao, S. Lu, K. Li, Y. Li, B. Yang, W. Chen, L. Wang, D. Li, H. Deng, F. Yi, and J. Tang, "Accelerated optimization of Ti_O2/Sb_2Se_3 thin film solar cells by high-throughput combinatorial approach," Adv. Energy Mater. **7**, 1700866 (2017).
[21]L. Guo, B. Zhang, S. Ranjit, J. Wall, S. Saurav, A. J. Hauser, G. Xing, L. Li, X. Qian, and F. Yan, "Interface engineering via sputtered oxygenated CdS:O window layer for highly efficient Sb_2Se_3 thin-film solar cells with efficiency above 7%," Solar RRL **3**, 1900225 (2019).
[22]P. Vidal-Fuentes, M. Guc, X. Alcobe, T. Jawhari, M. Placidi, A. Pérez-Rodríguez, E. Saucedo, and V. I. Roca, "Multiwavelength excitation raman scattering study of Sb_2Se_3 compound: fundamental vibrational properties and secondary phases detection," 2D Mater. **6**, 045054 (2019).
[23]A. Mavlonov, T. Razykov, F. Raziq, J. Gan, J. Chantana, Y. Kawano, T. Nishimura, H. Wei, A. Zakutayev, T. Minemoto, X. Zu, S. Li, and L. Qiao, "A review of Sb_2Se_3 photovoltaic absorber materials and thin-film solar cells," Sol. Energy **201**, 227 (2020).
[24]T. D. C. Hobson, O. S. Hutter, M. Birkett, T. D. Veal, and K. Durose, "Growth and characterization of Sb_2Se_3 single crystals for fundamental studies," in *2018 IEEE 7th World Conference on Photovoltaic Energy Conversion (WCPEC)* (2018) p. 0818.
[25]T. D. C. Hobson, L. J. Phillips, O. S. Hutter, K. Durose, and J. D. Major, "Defect properties of Sb_2Se_3 thin film solar cells and bulk crystals," Appl. Phys. Lett. **116**, 261101 (2020).
[26]C. A. Cody, L. DiCarlo, and R. K. Darlington, "Vibrational and thermal study of antimony oxides," Inorg. Chem. **18**, 1572 (1979).
[27]S. J. Gilliam, J. O. Jensen, A. Banerjee, D. Zeroka, S. J. Kirkby, and C. N. Merrow, "A theoretical and experimental study of Sb_4O_6: vibrational analysis, infrared, and raman spectra," Spectrochim. Acta A **60**, 425 (2004).
[28]V. L. Deringer, R. P. Stoffel, M. Wuttig, and R. Dronskowski, "Vibrational properties and bonding nature of Sb_2Se_3 and their implications for chalcogenide materials," Chem. Sci. **6**, 5255 (2015).